PERGAMON

International Journal of Heat and Mass Transfer 42 (1999) 2921–2933

International Journal of HEAT and MASS TRANSFER

Pulsed radial jet reattachment nozzle

D.L. James*, J.A. Castleberry, J.Y. Pak

Department of Mechanical Engineering, Texas Tech University, Lubbock, TX 79409-1021, U.S.A.

Received 13 January 1998; in final form 2 October 1998

Abstract

Steady periodic surface pressure distributions have been obtained for a mechanically pulsed radial jet reattachment (PRJR) nozzle. Local time-averaged and average Nusselt numbers have been obtained for air flow exiting a PRJR nozzle and impinging on a flat plate. The Nusselt numbers were obtained as a function of the following nondimensional nozzle parameters: Reynolds number, nozzle to plate spacing, exit angle, Strouhal number (pulsation frequency), exit gap spacing, and pulsation amplitude. The nozzle exit gap is cyclically varied for a PRJR nozzle, causing pulsations in the flow field that alter the convective coefficients and surface pressure distribution when compared to flow exiting an RJR nozzle under similar conditions. It was shown that the Nusselt number is a strong function of the Reynolds number, exit angle, and the combined effects of nozzle height, pulsation amplitude, and pulsation frequency.

Nomenclature

A Fourier coefficients
B Fourier coefficients
b nozzle gap
b_a gap variation, $b_{max}-b_{min}$
C constant
C_p pressure coefficient, $\frac{P_\infty - P_s}{\frac{1}{2}\rho \cdot U^2}$
H height, surface to top of gap
h convective heat transfer coefficient
k thermal conductivity
Nu Nusselt number, $\frac{h \cdot R_b}{k}$
P_s surface pressure on impingement plate
Pr Prandtl number
Q volumetric supply rate
q_o heat flux into the plate bottom
q_s heat flux from the plate surface
r radial distance from the nozzle centerline
R_b nozzle radius
R_s shaft radius
Re Reynolds number, $\frac{\rho \cdot U \cdot b}{\mu}$
St Strouhal number, $\frac{\frac{1}{2}\pi \cdot \omega \cdot b_a (R_b^2 - R_s^2)}{Q}$
T temperature
T_i sub-surface (internal) temperature
T_s surface temperature
T_∞ supply air temperature
U principle exit velocity, $\frac{Q}{2\pi \cdot R_b \cdot b}$
V voltage
UART Universal Asynchronous Receiver Transmitter
x sub-surface depth.

Greek symbols
α thermal diffusivity
Θ nozzle exit angle, declination beneath parallel to plate
μ dynamic viscosity
ρ density
ϕ crank (pulsation) phase angle
ω rate of pulsation.

1. Introduction

Many industries require the removal of heat and moisture in their daily operation. Examples include the pulp and paper industry, the agricultural industry, the food processing industry, as well as the electronics industry.

* Corresponding author. Tel.: 001 806 742 3563; fax: 001 806 742 3540; e-mail: darryl@thermal.me.ttu.edu

0017–9310/99/$ - see front matter
PII: S0017–9310(98)00359–7

Many of these operations involve pliable and semi-solid media, which are sensitive to deformation by the high surface forces that are typically coincident with high convective heat and mass transport. For certain configurations, the radial jet reattachment (RJR) nozzle has been shown to increase the convective heat and mass transfer coefficients while simultaneously reducing surface forces when compared to traditional in-line (circular) impinging jet nozzles [1].

Unlike in-line impinging jets, the flow from radial jets exits at some nearly-radial exit angle. Quiescent fluid is entrained into the jet's flow. As shown in Fig. 1, a flat surface beneath the radial jet forms a boundary that restricts the entrainment flow. For a certain range of conditions, this generates a low pressure region between the jet and the boundary which causes the jet's path to curve and eventually impinge onto the flat plate at some reattachment radius from the centerline. A theoretical analysis of laminar and turbulent radial jets [2] indicated the degree to which the radial jet would curve towards the plate. This analysis evaluated the dependence of RJR flow field parameters on nozzle parameters including exit angle, nozzle radius and height per exit gap, gap Reynolds number, and a turbulent spread parameter.

Outside the reattachment zone the flow forms into a radial wall jet with a developing momentum boundary layer. Inside the region bounded by the jet and the flat plate, the flow forms into a recirculating torroidal vortex. The existence of the torroidal vortex was numerically predicted by Lashefski et al. [3] and experimentally demonstrated by Agnew et al. [4].

Carbone's [5] experimental work investigated the effect of flow rates and nozzle geometries on the pressure coefficients on the impingement surface and the radial reattachment locations. The experimental results agreed with the theoretical result that for turbulent RJR, the reattachment radius and pressure coefficients are independent of the gap Reynolds number. A numerical investigation of laminar RJR by Lashefski et al. [6] agreed with the theoretical laminar RJR analysis that the flow field was dependent on the gap Reynolds number.

The radial jet impingement forms a reattachment zone, a circular ring around the centerline, characterized as a stagnation region. The local heat transfer rates on the surface of the plate are characterized by the three surface flow regions. The heat transfer rates are highest near the reattachment radius where the flow attaches to the flat plate. The heat transfer rates decrease outside the reattachment radius where the flow forms a radial wall jet with a thickening thermal boundary layer. Inside the reattachment radius the heat transfer rates are relatively low, owing to the recirculation of fluid in this region.

The heat transfer rates of in-line free jets were shown to be improved by intermittent flow pulsation frequencies in excess of a critical Strouhal number by Zumbrunnen and Aziz [7]. Conversely, in instances of sub-critical pulse rates, the pulsation of impinging in-line free jets can lead to reduced convective heat transfer. For sinusoidally pulsed in-line free jets, the heat transfer rates have been shown to be reduced by as much as 17% while square wave pulsations have been shown to increase the stagnation heat transfer coefficients by as much as 33% for Strouhal numbers greater than 0.26 [8]. It has been shown by Nevins and Ball [9] that for pulsed submerged in-line jets, the Nusselt number was independent of pulsation frequency (between 0 and 18 Hz) for sinusoidal, square, and triangular pulsed profiles. Castleberry and James [10] have presented results for a mechanically pulsed radial jet

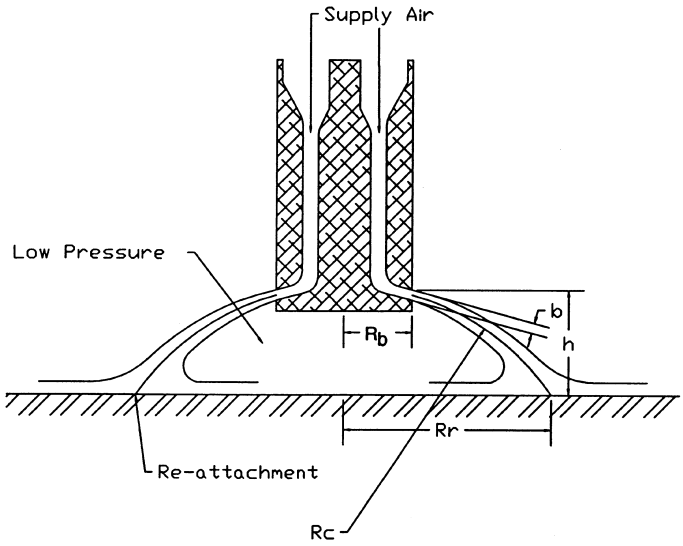

Fig. 1. RJR nozzle and typical flow pattern.

reattachment (PRJR) nozzle that show Nusselt number dependence on pulsation frequency (between 0 and 21 Hz), for fixed Reynolds numbers and pulsation amplitudes, for a submerged air jet.

Brittingham et al. [11] investigated the effects of single ramp-up or ramp-down variations in the incident flow velocity on the Nusselt number for impinging jets. Plots of the instantaneous Nusselt number were reported for various flow velocity disturbance duration ratios. Equivalent first order time constants were calculated for the instantaneous Nusselt number as a function of the nondimensional disturbance time.

In a numerical investigation of supply pulsed RJR, a limiting frequency was found to exist, above which the radial jet fails to reattach to the impingement surface. However experimental and k–ε numerical results did not agree due to periodic, non-axisymmetric blowouts that dominate the flow within the reattachment radius [4].

This paper presents an experimental investigation of a PRJR nozzle. In a PRJR nozzle, the nozzle exit gap is cyclically varied, causing pulsations in the flow field. The effect of amplitude and frequency of the mechanical pulsations on the heat transfer from a flat plate will be presented. Specific mechanisms that would cause an increase in heat transfer rates include (i) surging of the reattachment radius causing the location of the maximum heat transfer to sweep in and out, (ii) periodic destabilization of the flow field, leading to refreshing the fluid in the recirculating region, (iii) ejection of some portion of the recirculating fluid displaced by the nozzle diverter, (iv) increased mixing in the wall jet region and (v) periodic scouring of the boundary layer [9].

2. Experimental apparatus

A schematic overview of the PRJR nozzle apparatus components is shown in Fig. 2. At the center of the PRJR experimental apparatus was a 41.3 mm diameter nozzle with replaceable diverters and flow guides. Diverters and flow guides were made with -10, 0, 10, and 20° exit angles.

The nozzle assembly was mounted on the end of a 40.4 mm diameter tube, 15 diameters long. Close running fits in the lower guide and the upper guide/seal allow the shaft to move up and down. Nearly-sinusoidal pulsations of the radial gap are created by the rotation of a variable crank/connecting link mechanism driven by a DC motor with speed control/feedback by the acquisition computer.

Air for the nozzle is from the building compressed air supply. The air flows through a pressure regulator with a moisture separator, a settling tank, a solenoid valve, a metering value, one of two rotameters, past an RTD prove and then to the nozzle supply tube.

Two flat plates, one for the surface pressure measurements and one for the heat fluxes, were mounted in an X–Y traversing gantry. The gantry is moved by two stepper motors controlled by an 80286 based PC dedicated as a slave controller.

Pressure measurements were made using an Omega Engineering PX170, piezo-resistive bridge pressure transducer. The pressure transducer was installed beneath a single 0.7 mm diameter hole drilled through a 450 by 550 mm 16 gage flat plate.

The heat flux plate was made from mild steel bar cut, milled, and assembled to form a 260 by 400 mm plate 23 mm thick. Thermoplugs were installed into three holes bored through the plate. The thermoplugs were made from 6.4 mm diameter mild steel rod. Intrinsic thermocouple junctions were formed on the thermoplug by resistance welding 34 gage, type-T thermocouple wire onto the top and at 5 and 10 mm down the sides. The thermocouple junction on the top surface of the thermoplug was lapped down to be smooth with the top of the thermoplug. The top half of the thermoplug holes were overbored 0.2 mm. After installing the thermoplugs,

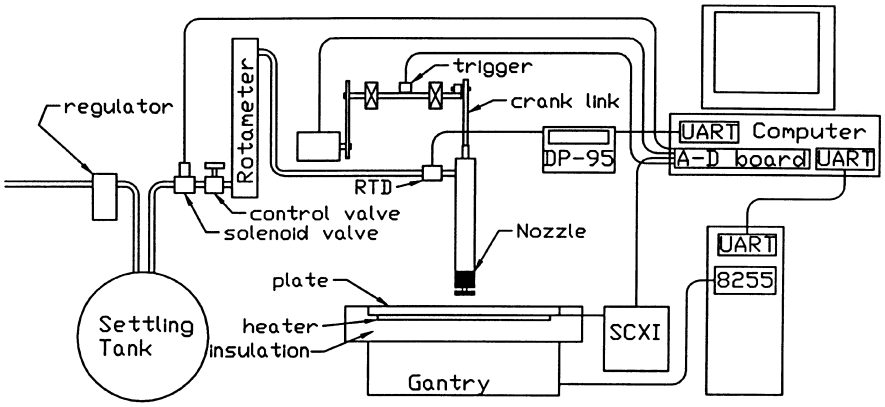

Fig. 2. Schematic of experimental setup.

the gap was filled with epoxy. A micro heat flux sensor manufactured by Vatell Corporation [12] was also installed in the heat flux plate. The heat flux sensor has a time constant of 6 ± 2 μs. The surface temperature and heat flux as measured by the micro heat flux sensor compared well with that measured with the thermoplugs at the same radial location. The heater mounted beneath the plate was a 254 by 360 mm, flexible rubber, electric heater rated at 15.5 kW m^{-2}. The heater was pressed against the underside of the plate by a backing of ceramic fiber insulation and a plate of 16 gage steel. The thermocouple wires were jacketed in a stainless steel overbraid to protect them physically and to shield them from the EM fields generated by the heater.

3. Experimental procedure

3.1. Pressure distribution

The data acquisition program would take 5000 measurements at a rate of 10 000 s^{-1} and record the resulting average. Twenty five cycles of data were acquired for the steady periodic surface pressure measurements, averaged, and recorded.

After data at each radial location had been obtained, a Fourier analysis was performed to fit the data. For each configuration, the first ten Fourier coefficients were calculated and used to plot the surface pressure distributions presented in the figurers in this paper. Pressure plots of the entire surface for two different PRJR nozzles were obtained. The pressure distribution in these plots were axisymmetric; therefore, for all remaining experiments, data was obtained for a single radial line extending outward from the nozzle centerline to several nozzle diameters.

3.2. Surface heat flux distribution

In order to determine the convective heat transfer coefficients, surface heat flux measurements were made. Prior to each heat flux measurement the heater and supply air were turned on until the temperature of the plate stabilized. Local surface heat fluxes were measured along a single radius extending out from the center line. The acquisition program moved the gantry to be a specified radial location, waited for thermal equilibrium to be established, scanned each thermocouple in the thermoplug 50 times and averaged. A Fourier analysis was performed to fit the data. At each location, the first four Fourier coefficients were calculated and used to record the surface temperature distributions as a function of the nozzle phase angle. The temperatures of the subsurface thermocouple scans were averaged over each cycle.

3.3. Analysis

Calibration of the pressure transducer over the gage pressure range of -550–550 Pa resulted in a linear relationship between the acquired voltage and the corresponding pressure. Calibration of all nine thermocouple channels also resulted in a linear equation that differed only in the offset relating the measured temperature and the true temperature [13].

The heat flux plate was modeled as a uniform, semi-infinite solid with a constant heat rate from beneath and the periodic surface temperature on the top as indicated in the following equation:

$$T_s = A_0 + \sum_{n=1}^{m} A_n \cos(n\omega t) + B_n \sin(n\omega t) \tag{1}$$

Additionally it was assumed that the thermophysical properties of the plate were constant, the problem was steady-periodic and one dimensional. The solution of this boundary value problem for the steady-periodic temperature distribution is given by equation (2),

$$T = A_0 + \frac{q''_o x}{k} + \sum_{n=1}^{m} \exp\left(-x\sqrt{\frac{n\omega}{2\alpha}}\right) \times \left[A_n \cos\left(n\omega t - x\sqrt{\frac{n\omega}{2\alpha}}\right) + B_n \sin\left(n\omega t - x\sqrt{\frac{n\omega}{2\alpha}}\right)\right] \tag{2}$$

where

$$A_0 = \frac{1}{m}\sum_{i=1}^{m} T_i \tag{3}$$

$$A_n = \frac{1}{m}\sum_{i=1}^{m} T_i \cos 2\pi nt \quad B_n = \frac{1}{m}\sum_{i=1}^{m} T_i \sin 2\pi nt. \tag{4}$$

This solution indicates that for the heat flux plate application, the 99% skin thickness was at most 5.04 mm. Because the heat flux plate was 23 mm thick the semi-infinite approximation was justified.

By differentiating the temperature distribution and evaluating the gradient at the surface, the instantaneous surface heat flux is given by:

$$q''_s = q''_o - k\sqrt{\frac{\omega}{2\alpha}} \times \left[\sum_{n=1}^{m} \sqrt{n}((A_n - B_n)\cos(n\omega t) + (A_n + B_n)\sin(n\omega t))\right] \tag{5}$$

The local instantaneous convective coefficient was calculated using:

$$h(r,t) = \frac{q''_s}{(T_{\text{surface}} - T_\infty)} \tag{6}$$

3.4. Uncertainty

Implicit in equation (6) is the assumption that the heat flux from the surface of the plate is entirely convective.

For typical conditions, the radiant heat transfer from the surface of the plate was approximately 200 W m^{-2}, corresponding to a typical total heat flux error of 2.8%.

The one-sigma standard deviation of the temperature measurements was found to be 0.17°C corresponding to ± 0.33°C at 95% confidence. Taking the average of 500 individual measurements reduced the temperature uncertainty to ± 0.015°C for 95% confidence.

Propagation of uncertainties in the values used in equation (6) were calculated and found to typically account for errors in the convective heat transfer coefficients of 4.5 W m^{-2} K^{-1}. In conjunction with the radiant losses the uncertainty for the steady state (average) heat transfer coefficients was typically $\pm 9.8\%$.

Uncertainties in the values used to evaluate the periodic heat flux in equation (5) typically resulted in errors of 450 W m^{-2}. Combined with concurrent steady error and radiant losses, the local instantaneous heat transfer coefficient had typical uncertainties of $\pm 13\%$ at 95% confidence.

The pressure measurement uncertainty was dominated by the gauge output uncertainty. The output uncertainty resulted in pressure measurement uncertainties of ± 14.1 Pa, or typically $\pm 5.6\%$ at 250 Pa. The rated time response of the gauge was 1 ms, and was not considered to be of consequence for the 5–30 Hz range of pulsation rates.

Uncertainties associated with the remainder of the apparatus included the air flow rate uncertainty of ± 0.7 CFM ($\pm 7\%$) at 10 cfm, the gantry positioning accuracy of ± 0.127 mm, the effective gauge location of ± 2.0 mm, the nozzle height uncertainty of ± 0.5 mm, and the nozzle to plate orthogonality to ± 1.0°. Refer to Castleberry [13] for the details of the uncertainty analysis.

4. Results and discussion

All experimental results obtained used air as the working fluid with Reynolds numbers based on the nozzle diameter varying between 1011 and 4149. The nozzle diameter was 41.3 mm. The turbulence intensities were measured for air exiting both RJR and PRJR nozzles at a Reynolds number of 1011 (smallest Reynolds number tested) using hot film anemometry at several locations throughout the flow field. The resulting turbulence intensities varied from a few percent to over one hundred percent; therefore the flow exiting each nozzle was turbulent.

4.1. Surface pressures

Surface pressure profiles and convective heat transfer coefficients were obtained as a function of non-dimensional nozzle height above the impingement surface H/R_b, nozzle exiting angle Θ, nozzle exit gap b/R_b, pulsation frequency ω, and nozzle phase angle ϕ. Because of the symmetry displayed in the 2D surface tests for both the PRJR and the RJR nozzle [13], all figures presented in this paper show data along a single radius extending outward from the nozzle centerline. Refer to Castleberry [13] for additional surface pressure plots.

The pressure distributions obtained for the PRJR nozzle show similarities and differences when compared to RJR pressure distributions. The pressure distributions as shown in Figs 3 and 4 plot the pressure coefficient, C_p, as a function of the non-dimensional radial position and the phase angle. A phase angle of zero represents the fully opened position (maximum gap spacing, minimum exit velocity), as the phase angle approaches 180° the nozzle stem is moving away from the impingement surface until at 180° the nozzle stem is at its most closed position (minimum gap spacing, maximum exit velocity). As the phase angle moves from 180 towards 360°, the stem is moving towards the impingement surface and the nozzle exit area is increasing.

For the case shown in Fig. 3, the pulsations were at the relatively low rate of 5 Hz ($St = 0.0051$). At this rate the location of the reattachment radius, the location of maximum pressure on the surface, changes very little in the radial direction. The pressure distribution within the reattachment radius is always sub-atmospheric as a result of the recirculating vortex located under the nozzle.

Figure 4 shows the transient, local surface pressures for the same configuration as shown in Fig. 3, but with pulsations at 19 Hz. At this higher rate, several dynamic effects can be seen. The radial position of the reattachment radius now moves radially in and out as a function of phase angle. In Fig. 4 it moves from a nondimensional radius of 1.64–2.11. This movement of the reattachment radius is due to the changing exit velocity and the changing volume beneath the pulsating diverter. It is also evident in Fig. 4 that the pressure distribution within the reattachment radius is not always sub-atmospheric as it is for the 5 Hz pulsation or for similarly configured RJR nozzles. There is no surface pressure indication of reattachment at phase angles near 270° (maximum rate of gap opening as the diverter is moving towards the impingement surface) indicating that the bulk movement of air under the nozzle at this instant is being pushed toward the impingement plate by the diverter. Another notable feature is this figure is that the pressure fluctuations propagate radially outward into the wall jet region as a result of the increased mixing caused by the higher frequency pulsation.

In general, as the frequency of pulsation increased, the maximum pressure increased in magnitude and lagged in phase. Movement of the reattachment radius increased as the ratio of maximum to minimum gap width increased, because the volume displaced underneath the diverter increased partially displacing the recirculating air radially outward. Negative exit angles produced smaller C_p mag-

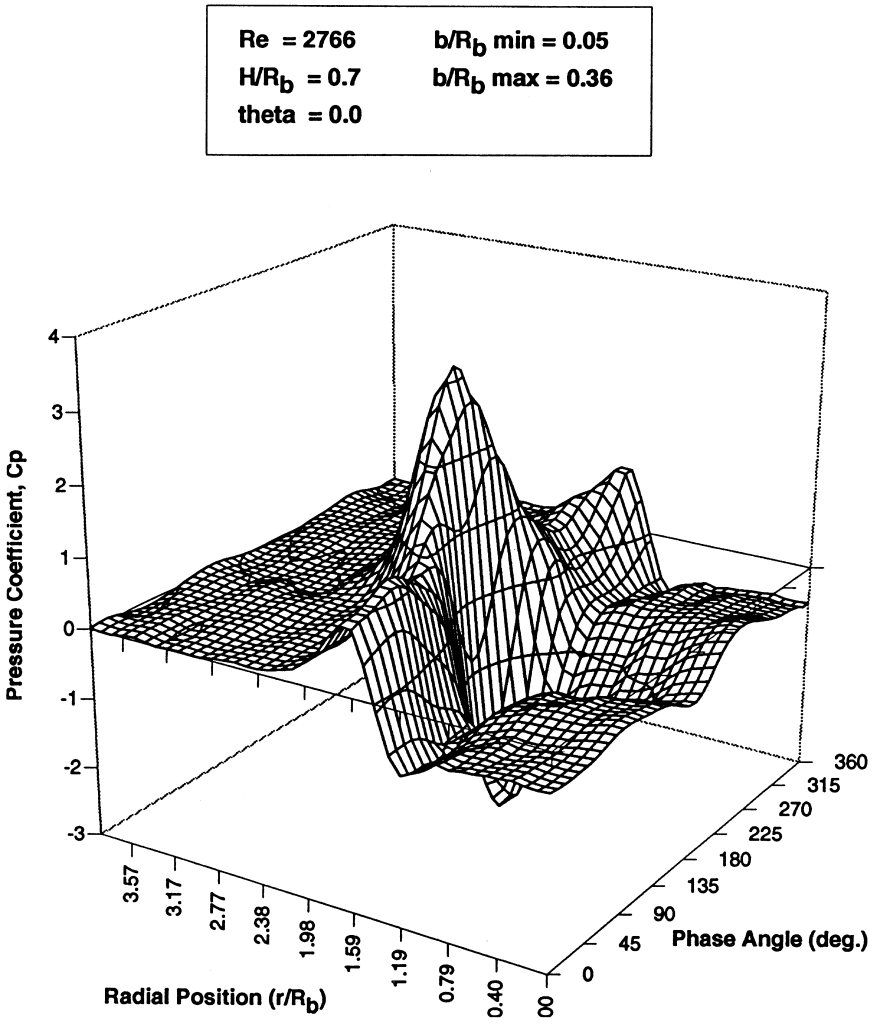

Fig. 3. PRJR surface pressure; pulsing frequency of 5 Hz ($St = 0.0051$).

nitudes, larger reattachment radii, and sub-atmospheric time and area averaged surface pressures.

4.2. Convective heat transfer coefficient

Convective heat transfer coefficients were obtained from both RJR and PRJR nozzles. The idea behind pulsing an RJR nozzle, thereby creating a PRJR nozzle, was to increase the local convective coefficients within the reattachment radius. A mechanical pulsing was employed in order to disrupt the recirculation region.

The local time-averaged heat transfer coefficient is related to the local, instantaneous coefficient by

$$\overline{h(r)} = \frac{1}{2\pi}\int_0^{2\pi} h(r,\phi)\mathrm{d}\phi \tag{7}$$

The average convective coefficient reported in each figure represents the average convective coefficient for the entire area given in the respective plot. The average heat transfer coefficient as defined by Chyu [14] was utilized, giving:

$$\bar{h} = \frac{1}{A}\int_{r=0}^{R} \overline{h(r)}\, 2\pi r\, \mathrm{d}r \tag{8}$$

Before a discussion on the experimental results, it is important to explain the information found in the figures that present local, time-averaged convective coefficients. The information found in each of these figures contains the Reynolds number (Re), nondimensional exit angle (theta), the nondimensional height (H/R_b), and the maximum and minimum exit gap height (b/R_b). The nondimensional pulsation amplitude is obtained by taking the difference between b/R_b max and b/R_b min. The local, time-averaged convective coefficients obtained for the PRJR nozzle are plotted for a minimum of three different

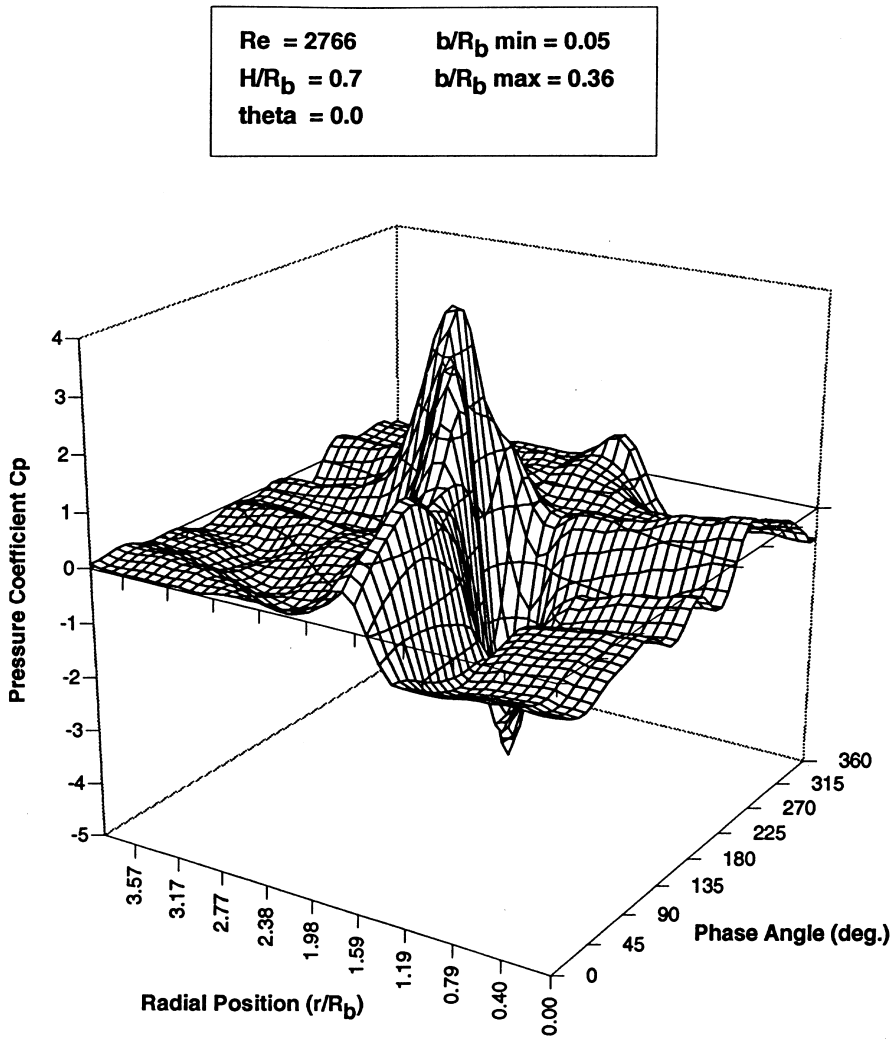

Fig. 4. PRJR surface pressure; pulsing frequency of 19 Hz ($St = 0.0192$).

frequencies. On several of the figures presented, convective data is presented for an RJR nozzle for comparative purposes. The RJR nozzle data corresponds to either the maximum (b/R_b max), the minimum (b/R_b min), or the average nondimensional gap spacing ((b/R_b min$+b/R_b$ max)/2). In addition, average convective coefficient values are reported based on the radial distance given in each figure and are listed as '*Nu* avg' in each legend.

4.2.1. Local, time-averaged results

Changing the Reynolds number of the air exiting the PRJR nozzle greatly affected the local, time-averaged heat transfer coefficient as can be seen in Figs 5–7 when all other parameters were held constant; $H/R_b = 0.8$, b/R_b min $= 0.05$, $\Theta = 0$, nondimensional pulsation amplitude $= 0.31$. For example, the maximum PRJR heat transfer coefficient shown in Fig. 7 ($Nu_{max} \approx 112$ at 20 Hz), corresponding to a Reynolds number of 3873 is approximately 100% larger than the maximum coefficient shown in Fig. 6 ($Nu_{max} \approx 55$) and 300% larger than that shown in Fig. 5 ($Nu_{max} \approx 35$), where the Reynolds numbers were 1936 and 1011, respectively. Simply put, as the Reynolds number increased, the jet had less time to lose momentum to the surroundings resulting in a greater maximum heat transfer coefficient at the reattachment location. Although the increased convective coefficients for increased Reynolds number is intuitive for the positive exit angles, it is not so intuitive for the negative exit angle tested. The reason that the negative 10° exit angle case behaves similar to the other angles tested is that the low pressure region of the toroidal vortex located between the reattachment radius and the bottom of the nozzle pulls the jet toward the

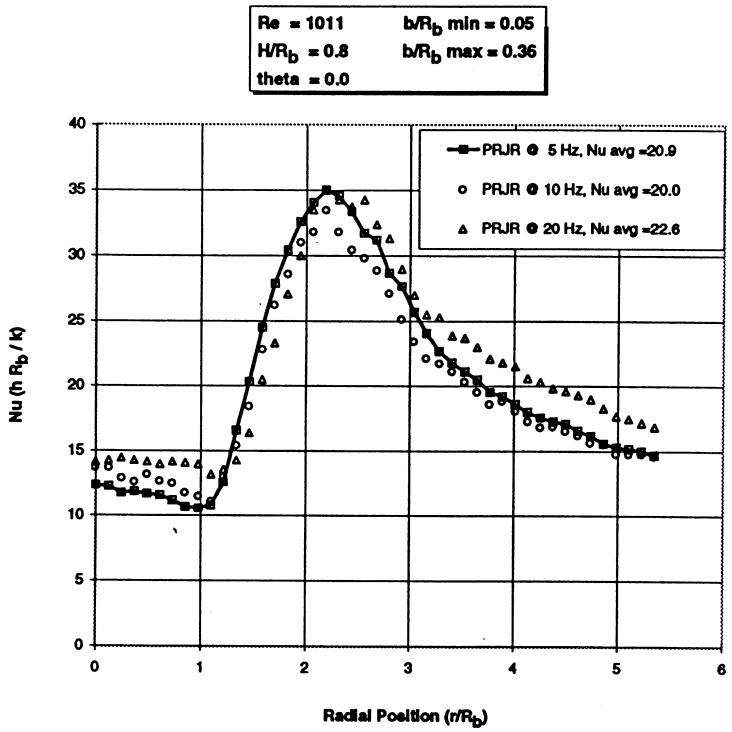

Fig. 5. Local, time-averaged convective coefficients from a PRJR nozzle; *St* 0.0166 (5 Hz), 0.0304 (10 Hz), and 0.0581 (20 Hz).

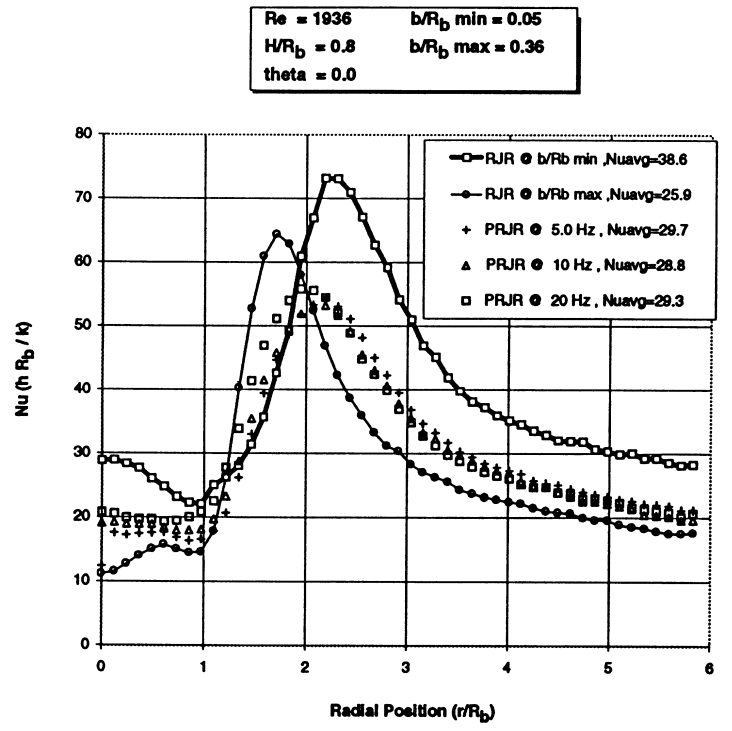

Fig. 6. Local, time-averaged convective coefficients from PRJR and RJR nozzles; *St* 0.0072 (5 Hz), 0.0143 (10 Hz), and 0.0289 (20 Hz).

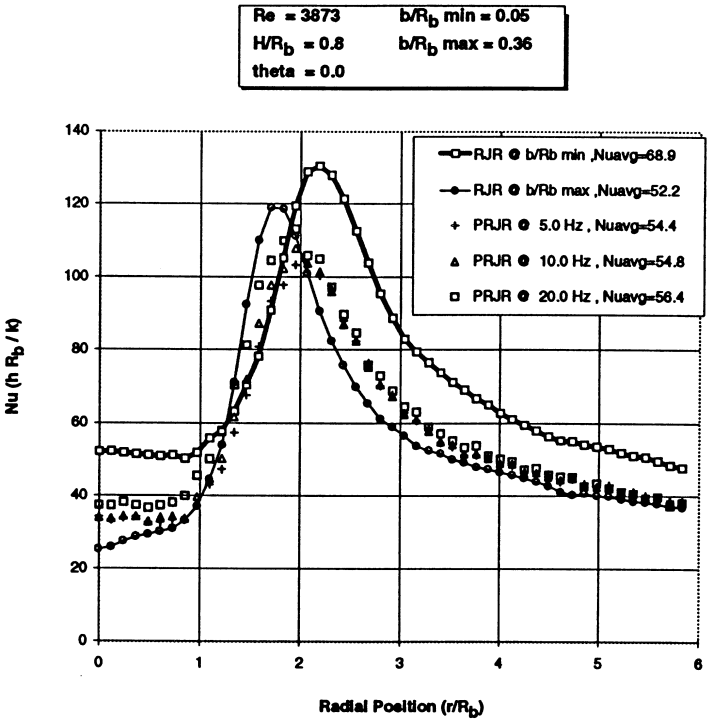

Fig. 7. Local, time-averaged convective coefficients from PRJR and RJR nozzles; *St* 0.0036 (5 Hz), 0.0071 (10 Hz), and 0.0144 (20 Hz).

impingement surface. In other words, the strength of the vortex compensates for the fact that the jet discharges with higher momentum angled away from the impingement surface. The vortex is created as the fluid located beneath the nozzle is entrained into the jet's flow. The flat plate beneath the radial jet restricts the entrainment flow thus generating a low pressure region between the jet and the surface which causes the jet's path to curve and eventually impinge onto the flat plate at some reattachment radius from the centerline.

The location of the effective reattachment radius changed very little as the frequency of pulsation was varied as is evident in each of Figs 5–7. The location of the reattachment radius does change positions radially as illustrated in the instantaneous pressure plots, however, after time-averaging over one period, the location of the effective reattachment radius is relatively independent of pulsation frequency. Also of note, for the range of pulsing frequencies tested, the maximum local time-averaged convective coefficient from the PRJR nozzle typically fell below the maximum convective coefficient from one of the RJR nozzle cases tested. The average heat transfer coefficient for the PRJR data typically fell between the averaged RJR data corresponding to the maximum and minimum gap openings as illustrated in Figs 6 and 7.

The effect of exit angle on the convective coefficient can be seen in Figs 8–10. The data in these figures represent all parameters held constant expect the exit angle that was varied from -10 to $+20^\circ$. An exit angle of 0° corresponds to the nozzle stem diverting the exiting air jet parallel to the impingement surface. Positive angles represent the air jet exiting toward the plate, whereas the negative angle diverts the air jet away from the plate. The maximum Nusselt number decreased by nearly 47%, from 90 to 48, and the effective reattachment radius moved from r/R_b equal to approximately 1.6–2.5 as the exit angle changed from $+20^\circ$, Fig. 10, to -10°, Fig. 8 for the PRJR nozzle. The trends of increasing heat transfer coefficients and decreasing reattachment radius were observed in all the cases tested for the PRJR nozzles as the exit angle became more positive. Unseen in the figures presented, but the reason for the changing reattachment radius, convective data, and surface pressure is the toroidal vortex underneath the nozzle and the corresponding low pressure region that is responsible for the curvature of the jet as it leaves the nozzle and moves toward the impingement surface. The vortex is larger for the -10° exit angle and becomes smaller as the exit angle changes to positive angles.

Changing the nozzle height above the impingement surface led to some interesting results for the PRJR nozzle. When all other parameters were held constant

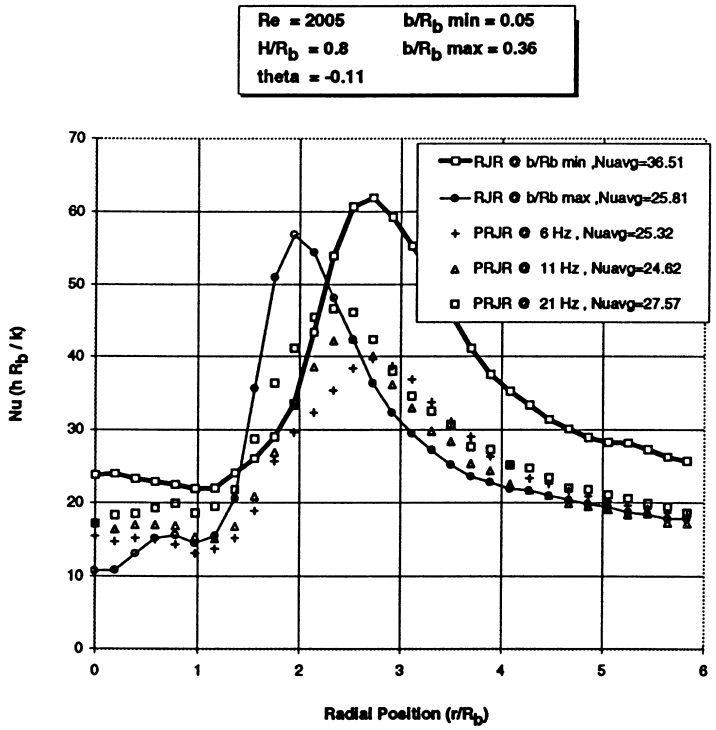

Fig. 8. Local, time-averaged convective coefficients from PRJR and RJR nozzles; *St* 0.0084 (6 Hz), 0.0153 (11 Hz), and 0.0293 (21 Hz).

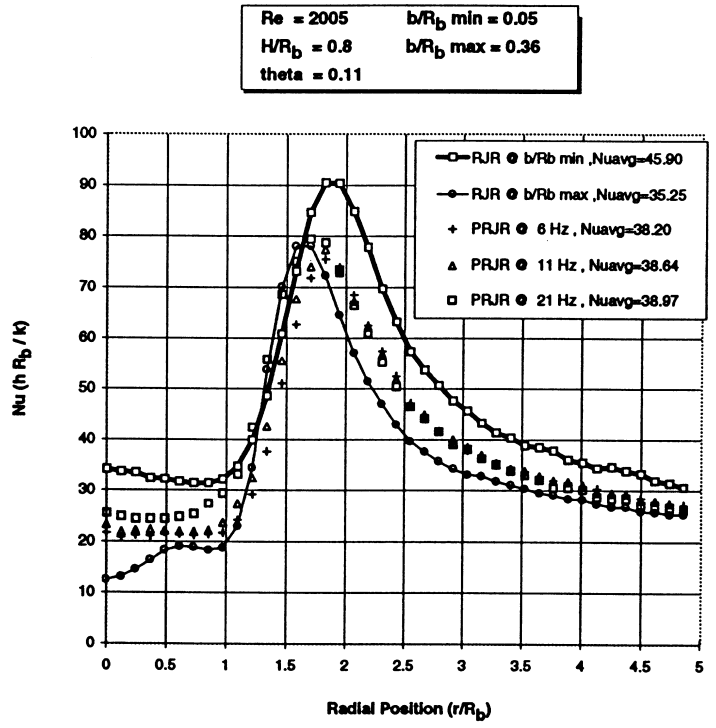

Fig. 9. Local, time-averaged convective coefficients from PRJR and RJR nozzles; *St* 0.0084 (6 Hz), 0.0153 (11 Hz), and 0.0293 (21 Hz).

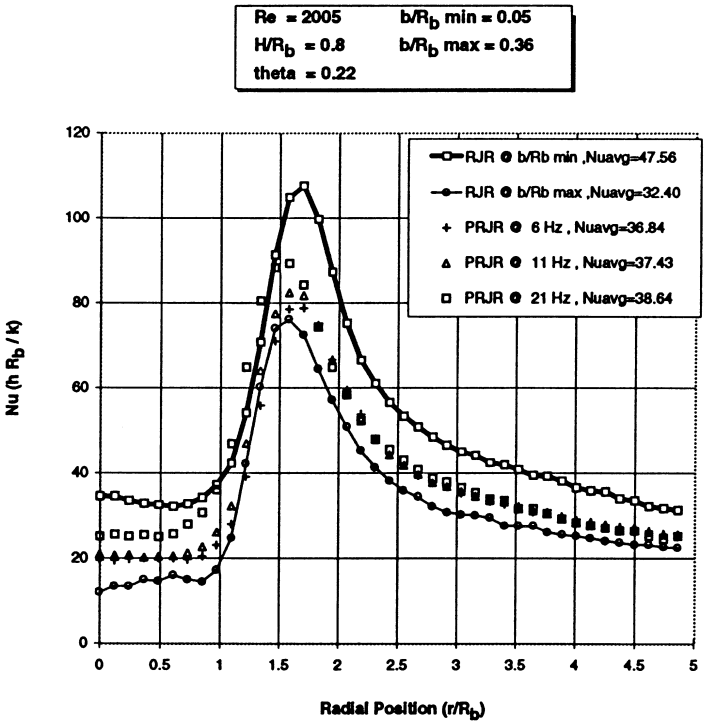

Fig. 10. Local, time-averaged convective coefficients from PRJR and RJR nozzles; *St* 0.0084 (6 Hz), 0.0153 (11 Hz), and 0.0293 (21 Hz).

and the Reynolds numbers was low (2005 or less), as the nozzle height, H/R_b, was changed from 1.3–0.8, the conditions that gave the maximum heat transfer coefficients for the PRJR nozzle at the farthest position, did not produce the maximum heat transfer when the PRJR nozzle was located at the closest position to the impingement surface. Figure 11 shows that when the nozzle height was located at a nondimensional position of 1.3, the lowest pulsation frequency produced the highest convective heat transfer coefficient, independent of the pulsation amplitudes and minimum gap openings tested. However, for a nondimensional nozzle height of 0.8, the largest pulsation frequency coupled with the large pulsation amplitude, but independent of the minimum gap opening, produced the highest convective heat transfer coefficient as can be seen in Figs 6–10.

The reason for this unique behavior is that the PRJR nozzle behavior approaches an RJR nozzle for low pulsation rates coupled with the larger nozzle-to-plate spacing. The rate of change in volume under the nozzle or in the discharge velocity is not significant enough to produce changes near the reattachment region. In contrast, for the higher pulsation rates and the smaller nozzle-to-plate spacing, the rate of change of volume under the nozzle causes the reattachment radius to move to and fro effectively increasing the area of the greatest heat transfer that occurs at the reattachment location.

Testing the PRJR nozzle at a Reynolds number near 4000, the trends described previously did not hold for all exit angles. For the cases of the positive 10 and 20° exit angles, the higher pulsation rates produced the highest convective coefficient no matter the nozzle height or the minimum gap opening, as can be seen in Fig. 12. At higher Reynolds numbers, tests would have needed to be conducted at greater nozzle-to-plate spacing than were tested for the behavior described previously to occur as the time for the air leaving the nozzle and impinging upon the plate should remain constant.

5. Conclusions

Surface pressure distributions have been determined for air exiting a PRJR nozzle and impinging on a flat plate. The time-averaged surface pressure distributions show that the area within the reattachment radius is generally subatmospheric for the range of parameters investigated; however for some PRJR nozzle configurations, there existed small regions within the reattachment radius that have a pressure greater than atmospheric for very small periods of time. In general, as the frequency of pulsation increased, the maximum pressure increased in magnitude and lagged in phase. Movement of the reattachment radius increased as the

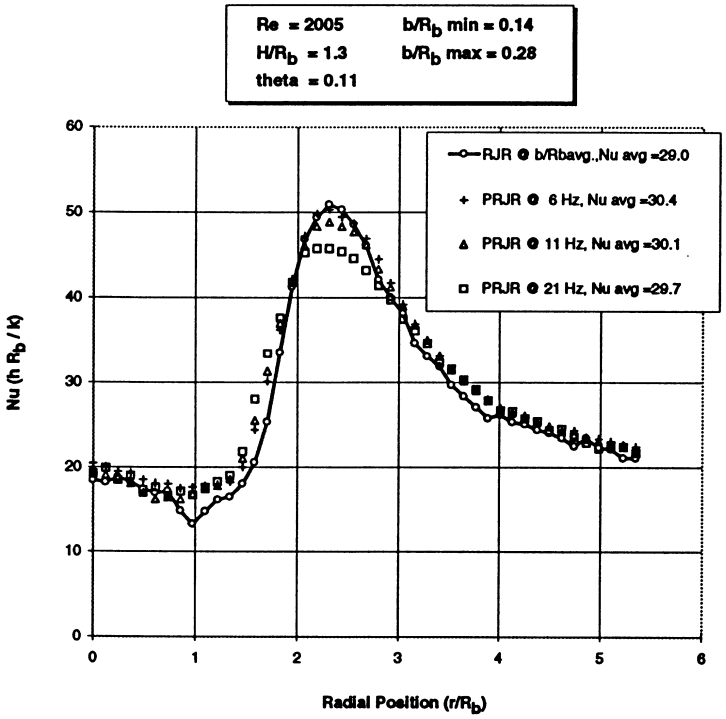

Fig. 11. Local, time-averaged convective coefficients from PRJR and RJR nozzles; *St* 0.0038 (6 Hz), 0.0069 (11 Hz), and 0.0132 (21 Hz).

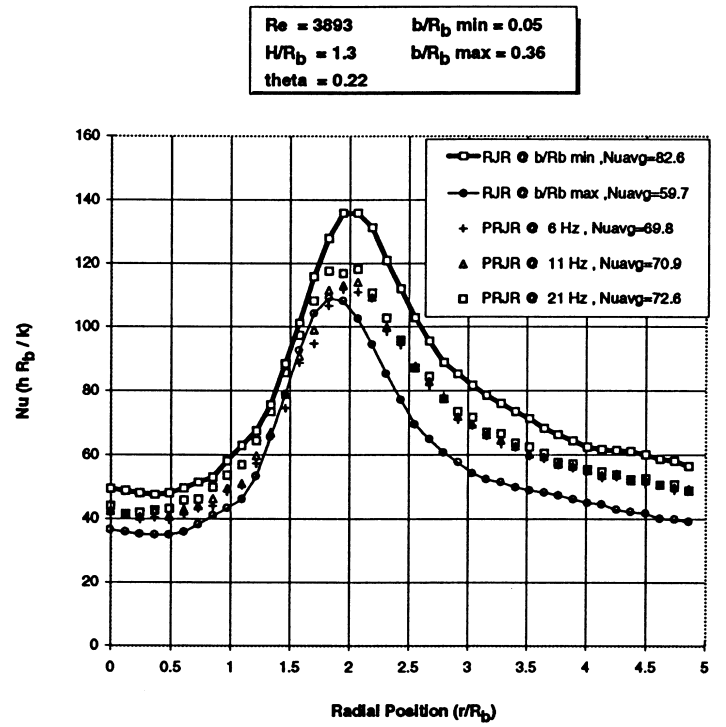

Fig. 12. Local, time-averaged convective coefficients from PRJR and RJR nozzles; *St* 0.0042 (6 Hz), 0.0077 (11 Hz), and 0.0147 (21 Hz).

ratio of maximum to minimum gap width increased, because the volume displaced underneath the diverter increased partially displacing the recirculating air radially outward; negative exit angles produced small C_p magnitudes, larger reattachment radii, and subatmospheric time and area averaged surface pressures.

Local time-averaged and average heat transfer coefficients, in the form of Nusselt numbers, were determined for air exiting a PRJR nozzle and impinging upon a flat plate. The time-averaged convective coefficients have been shown to be strongly dependent upon the Reynolds number, exit angle, and the combined effects of nozzle height, pulsation amplitude, and pulsation frequency. Heat transfer increased as the Reynolds number increased, as the exit angle became more positive, and as the nozzle height decreased. For Reynolds numbers of 2005 or less, the higher pulsation frequencies produced larger convective coefficients when the nozzle was positioned close to the surface ($H/R_b = 0.8$) and the larger pulsation amplitude was employed. In contrast the lower pulsation frequencies produced larger convective coefficients when the nozzle was positioned at the greatest height tested ($H/R_b = 1.3$), independent of the pulsation amplitude as the PRJR nozzle behaved like an RJR nozzle.

Of the specific mechanisms that were initially identified for effecting the heat transfer rates for the nozzle parameters tested, surging of the reattachment radius causing the location of the maximum heat transfer to sweep in and out, ejection of some portion of the recirculating fluid displaced by the nozzle diverter, and increased mixing in the wall jet region have been identified in this paper.

It is possible for the average convective coefficient from the PRJR nozzle to at least equal, and possibly exceed, that from a similarly configured RJR nozzle; however, for most of the cases tested and all the cases presented in this paper the average heat transfer coefficient from the PRJR nozzle was less than the maximum average heat transfer coefficient from the similarly configured RJR nozzle.

The engineering decision concerning which set of nozzle parameters to choose is dependent upon the application and the tradeoff between surface forces and convective heat transfer. Subatmospheric area-averaged surface forces and the smallest averaged heat transfer coefficients corresponded to the negative exit angle, whereas positive area-averaged surface forces, although still small (less than 1 N over 19 600 mm^2) and larger convective coefficients occurred for the $+20^\circ$ exit angle.

Acknowledgement

The authors would like to express gratitude to the Center for Energy Research, Texas Tech University for financial support of this work.

References

[1] J. Seyed-Yagoobi, V. Narayanan, R. Page, Comparison of heat transfer characteristics of radial jet reattachment nozzle to in-line impinging jet nozzle, Journal of Heat Transfer 120 (1998) 335–341.
[2] R. Page, L. Hadden, C. Ostowari, Theory for radial jet reattachment flow, AIAA Journal 27 (11) (1989) 1500–1505.
[3] H. Lashefski, A. Holl, A. Grosse-Gorgemann, N. Mitra, R. Page, Flow structure and heat transfer of radial and axial jet reattachment on a flat plate, Fundamentals of Forced Convective Heat Transfer, HTD 210 (1992) 123–131.
[4] N. Agnew, D. Elvery, K. Bremhorst, Modeling of a steady and a fully pulsed reattaching radial jet, Proceedings of Eleventh Australasian Fluid Mechanics Conference, Hobart, Australia, (1992) 1097–1100.
[5] J. Carbone, Flow field characteristics of a radial jet reattaching on a flat plate. Master's thesis, Texas A&M University, 1988.
[6] H. Lashefski, T. Cziesla, N. Mitra, Influence of exit angle on radial jet reattachment and heat transfer, Journal of Thermophysics and Heat Transfer 9 (1) (1995) 169–174.
[7] D. Zumbrunnen, M. Aziz, Convective heat transfer enhancements due to intermittency in an impinging jet, ASME Journal of Heat Transfer 115 (1993) 91–98.
[8] H. Sheriff, D. Zumbrunnen, Effect of flow pulsations on the cooling effectiveness of an impinging jet, ASME Journal of Heat Transfer 116 (1994) 886–895.
[9] R. Nevins, H. Ball, Heat transfer between a flat plate and a pulsating impinging jet, Proceedings of the National Heat Transfer Conference, Boulder, CO, 1961, pp. 510–516.
[10] J. Castleberry, D. James, Pulsed radial jet reattachment nozzle heat transfer to a flat plate, Proceedings of National Heat Transfer Conference, AICHE Symposium Series, Baltimore, MD, 1997, pp. 282–287.
[11] R. Brittingham, E. Mladin, D. Zumbrunnen, Heat transfer transients in stagnation flows due to changes in flow velocity, Journal of Thermophysics and Heat Transfer 10 (1) (1995) 186–189.
[12] Vatell Corporation, Model HFM 6-C/H. Christiansburg, VA.
[13] J. Castleberry, Heat transfer and surface pressure measurements for air exiting a pulsed radial jet reattachment nozzle. Master's thesis, Texas Tech University, 1997.
[14] M. Chyu, On the boundary condition and data reduction of heat transfer experiment, International Communications in Heat and Mass Transfer 14 (5) (1987) 543–550.